High-strength magnetic hydrogels with photo-weldability made by stepwise assembly of magnetic-nanoparticle-integrated aramid nanofiber composites

Zuochen Wang‡†,[1,2] Hengjia Zhu‡,[1] Hegeng Li,[1] Zhisheng Wang,[3] Mingze Sun,[1] Bin Yang,[1,2] Yufeng Wang,[3] Liqiu Wang,[1,4] and Lizhi Xu[1,2]*

[1]Department of Mechanical Engineering, The University of Hong Kong, Hong Kong SAR 999077, China.

[2]Advanced Biomedical Instrumentation Centre Limited, Hong Kong SAR 999077, China.

[3]Department of Chemistry, The University of Hong Kong, Hong Kong SAR 999077, China.

[4]Department of Mechanical Engineering, The Hong Kong Polytechnic University, Kowloon, Hong Kong SAR 999077, China.

ABSTRACT: Hydrogels capable of transforming in response to magnetic field hold great promise for applications in soft actuators and biomedical robots. However, achieving high mechanical strength and good manufacturability in magnetic hydrogels remains challenging. Here, inspired by natural load-bearing soft tissues, a class of composite magnetic hydrogels is developed with tissue-mimetic mechanical properties and photothermal welding/healing capability. In these hydrogels, a hybrid network involving aramid nanofibers, magnetite Fe_3O_4

nanoparticles, and polyvinyl alcohol is accomplished by a stepwise assembly of the functional components. The engineered interactions between nanoscale constituents enable facile materials processing and confer a combination of excellent mechanical properties, magnetism, water content and porosity. Furthermore, the photothermal property of Fe_3O_4 nanoparticles organized around the nanofiber network allows near infrared welding of the hydrogels, providing a versatile means to fabricate heterogeneous structures with custom designs. Complex modes of magnetic actuation are made possible with the manufactured heterogeneous hydrogel structures, suggesting opportunities for further applications in implantable soft robots, drug delivery systems, human-machine interactions, and other technologies.

KEYWORDS: biomimetic materials, magnetic hydrogels, NIR-welding, nanofibers, porous, soft actuators

INTRODUCTION

The burgeoning field of soft robotics calls for advanced materials that can be actuated in response to external stimuli.[1–7]Among the variety of soft active materials, magnetic hydrogels are particularly useful for biomedical applications.[3,8–10] They are water-rich, biocompatible, and tailorable in mechanical properties. With assistance of high magnetization nanoparticles, they can be remotely manipulated through biocompatible low-intensity magnetic field, allowing for safe operation in living organisms. Magnetic hydrogels could be implemented in advanced tools for drug delivery,[11] tissue engineering platforms,[12] human-machine interactions,[2] and many other technologies. However, existing magnetic hydrogels exhibit limited mechanical strength and manufacturability, which restrict their practical applications.[1,13] Indeed, the required inorganic magnetic components often disrupt the structural properties of hydrogels that highly rely on the

porous network of polymers.[14] On the other hand, the complex synthesis schemes for mechanically strong hydrogels might not be compatible with functional design of the composites or fabrication of hybrid device structures.[15–17]

In biological soft tissues, such as skin, blood vessels, ligaments, *etc*., an excellent combination of mechanical properties, functionality and water retention was accomplished with the hybrid nanofiber networks involving collagen and other soft biopolymers.[3,8,18,19] They provide a robust structural basis for various physiological functionalization, allowing for the formation of heterogeneous organs that operate under dynamic mechanical deformation. Emulating these features of natural soft tissues would enable a versatile materials platform for the construction of reliable functional structures for advanced bio-integrated systems. However, it remains difficult due to the limited synthetic building blocks.

Recently emerged nanocomposites based on aramid nanofibers (ANFs) indicate a new route for the engineering of magnetic hydrogels that could address these challenges.[8,20–23] ANFs self-assemble into 3D networks that exhibit microstructural properties similar to those of natural collagen fibers, providing a biomimetic framework for the construction of various soft composites.[8] The polar groups on ANFs allow interactions with other organic materials, facilitating the formation of functional hydrogels that retain the high structural robustness arising from the nanofiber skeleton.[20,24] Nevertheless, incorporation of magnetic components in the ANF network is still difficult. For instance, in-situ synthesis of magnetic nanostructures highly relies on surface chemistry, wherein the functional groups determine nanoparticle nucleation and growth. Due to the chemical stability of para-aramid (poly (p-phenylene terephthalamide)) (PPTA) chains, chemical modification of ANFs requires complex and cumbersome procedures that might not be compatible with magnetic components.[22] Physical deposition methods,[23,25,26]

including vacuum assisted filtration and matrix infiltration, require diffusion of functional building blocks in aqueous or vapor phase. In the presence of the significant interactions between magnetic particles, these processes may cause severe aggregation or non-uniform distribution of the particles, leading to compromised functionality or structural failure by stress concentration. Therefore, developing strategies for reliable incorporation of magnetic components into ANF-based composites hydrogels becomes essential.

Herein, we report a facile fabrication strategy for ANF-based magnetic hydrogels with high mechanical strength and excellent manufacturability. Magnetite Fe_3O_4 nanoparticles functionalized with alkyl chains terminated with amine ($-NH_2$) groups exhibit good stability in suspension while enabling desired interactions with ANFs. Stepwise assembly of ANFs, Fe_3O_4 nanoparticles, and polyvinyl alcohol (PVA) *via* solution-based mixing processes leads to magnetically responsive nanofiber network with excellent structural robustness and uniformity. In addition, photothermal property of Fe_3O_4 nanoparticles and the reconfigurable hydrogen bonding within the nanofiber hydrogels affords fast and reliable welding with near infrared (NIR) radiation[27–30]. Alternatively, functional moiety such as nanoparticles or organic dyes[31] dispersed in the composites, might enable selective welding *via* laser irradiation. However, the use of noble nanoparticles as functional components dramatically increases the cost, whereas the organic dye molecules cannot sustain the high temperature required to soften the polymer composites. The use of Fe_3O_4 nanoparticle in the composite hydrogels is particularly beneficial since it enables photothermal effects without additional components. NIR-laser-based photothermal welding enables production of Janus-type hydrogel structures or other complex and heterogeneous patterns, which allows for various modes of magnetic actuation with custom

designs. The nanofibrous magnetic hydrogels also exhibit good biocompatibility, indicating potential applications in bio-integrated device systems.

RESULTS AND DISCUSSION

Synthesis of the ANF-Fe_3O_4-PVA hydrogels. To fabricate composite hydrogels with desirable properties in bulk, a stepwise assembly strategy is employed (Figure 1a). Preparation of the composite hydrogel starts with intermixing the colloidal suspensions of Fe_3O_4-NH_2 nanoparticles and ANFs in dimethyl sulfoxide (DMSO). The hydroxyl and amine groups on the magnetite nanoparticles allow spontaneous packing with the ANFs *via* hydrogen bonding. The DMSO suspension of ANF-Fe_3O_4 is then mixed with DMSO solution of PVA, which will further enhance stretchability and toughness of the nanofiber networks.[8] The ternary mixture appears a viscous and moldable fluid (Figure S1), since DMSO is a strong hydrogen bonding acceptor and prevent unwanted gelation at this stage. After the mixing steps, a solid hydrogel can be obtained when the mixture is immersed in water, wherein DMSO is exchanged by water, a weaker hydrogen bond acceptor.[8]

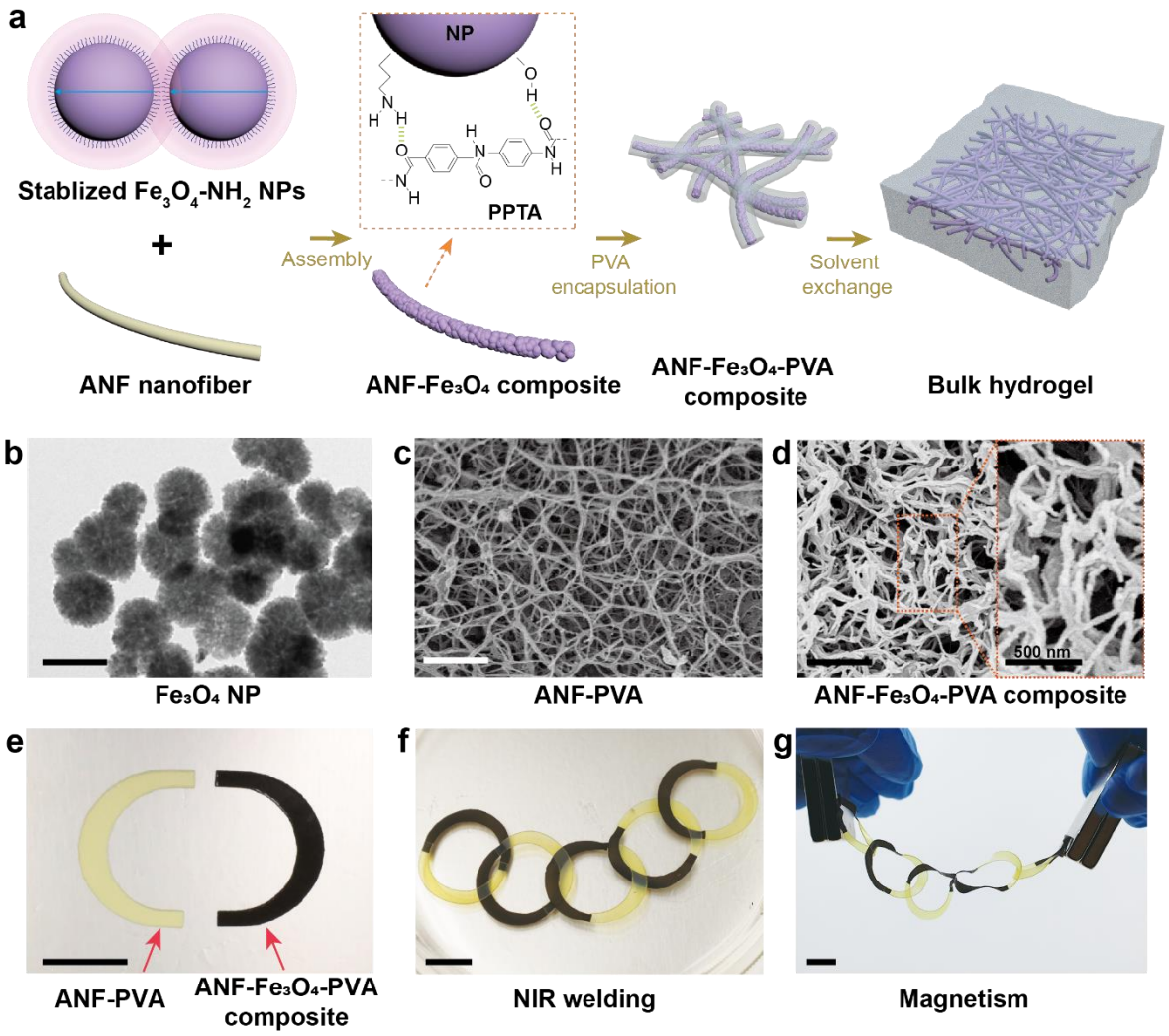

Figure 1. Tough and stretchable magnetic hydrogels stemming from hyper-connective ANF composites. (a) Schematics showing formation process of the hierarchical structures. The surface ligand plays an essential role in stabilizing the magnetic nanoparticle against strong dipolar interactions. (b) TEM image showing Fe_3O_4-NH_2 nanoparticles, where the aggregation was induced by drop casting method using DI water. Scale bar: 200 nm. (c-d) SEM images showing the morphology of (c) ANF-PVA hydrogel and (d) ANF-Fe_3O_4-PVA composite hydrogel after critical point drying, where the nanoparticles are embedded on the surface of the nanofibers. Scale bars: 1 μm. (e) Photograph showing as-fabricated ANF-PVA (left) and ANF-Fe_3O_4-PVA

(right) composite hydrogels. (f) Photograph showing NIR welded hydrogel sample. (g) Photograph showing programed magnetic response of the sample. Each magnet used has dimensions of 40 × 60 × 5 mm, with center magnetic field strength of 40 mT and edge magnetic field strength of 160 mT. Scale bars: 10 mm.

To match the diameter of the nanofibers, we synthesized Fe_3O_4 nanoparticles with diameters of ~25 nm.[24] The nanoparticles are surface functionalized with alkyl chains terminated with amine and hydroxyl groups (Figure 1b). The magnetite Fe_3O_4 lattices were further verified by X-Ray diffraction (Figure S2), vibrating-sample magnetometer (Figure S3a), and transmission electron microscopy (TEM) ring diffraction pattern (Figure S4), which is consistent with theoretical calculations based on the reported lattice parameters (Table S1). A superparamagnetic response with maximum of 74 emu/g was achieved for Fe_3O_4 nanoparticles. Besides controlling the size of nanoparticles using hydrothermal synthesis, there are other strategies to manipulate the morphology and composition of the magnetic nanoparticles, leading to high saturation magnetization for operation under weak magnetic field.[9] For instance, thermal decomposition methods, introducing shape anisotropy, or adding zinc or cobalt elements[32–34] may be considered depending on the functional requirement of the material system. During synthesis of Fe_3O_4 nanoparticles, 1,6-hexanediamine was used as the modulator, which helps to control the size of the particles and produces sufficient alkyl chains terminated with amine groups on their surfaces. In deionized (DI) water, the surface alkyl chains closely pack on the surface of Fe_3O_4-NH_2 nanoparticles due to their poor solubility in water. The dissociation of amine and hydroxyl groups is thus limited, producing weak electrostatic repulsion between nanoparticles. The nanoparticles aggregate due to dominated dipolar and van der Waals attractions and settle to the bottom of glass vials within seconds (Figure S5), which contrasts with highly charged Fe_3O_4-

COOH particles (Figure S6). However, in an organic solvent such as DMSO, the alkyl chains are highly dissolved and solvated. The steric repulsion of Fe_3O_4-NH_2 nanoparticles counteracts the dipolar attraction or van der Waals interactions, forming stable colloidal suspension (Figure 1a & S6b).

Scanning electron microscopy (SEM) shows the microscale morphology of the ANF-Fe_3O_4-PVA hydrogels. The Fe_3O_4 nanoparticles attached to the nanofibers without significant aggregation or disruption of the 3D interconnected network (Figure 1c-d). It is conceivable that the nanofiber network provides an excellent template to guide the assembly of Fe_3O_4 nanoparticles and acts as a robust structural framework to bear mechanical loads. We fabricated hydrogels with four different concentrations of loaded Fe_3O_4 nanoparticles (7.3 wt%, 13.7 wt%, 24.1 wt%, and 32.2 wt%) denoted as ANF-Fe_3O_4-PVA-1 to ANF- Fe_3O_4-PVA-4. The magnetic response can be adjusted through controlling the composition of the hydrogel without major influence on the superparamagnetic properties of nanoparticles (Figure S3b-c). In addition, due to the inherent magnetic and photothermal properties of Fe_3O_4 nanoparticles, the ANF-Fe_3O_4-PVA and ANF-PVA hydrogels can be further processed with NIR welding to form hybrid structures with designed magnetic responses (Figure 1e-g).

Mechanical properties of the ANF-Fe_3O_4-PVA hydrogels. Due to the hybrid nanofiber network,[20,35]ANF-Fe_3O_4-PVA hydrogels are mechanically strong and stretchable (Figure 2a-b). To quantitatively analyze their mechanical properties, we performed tensile and compression tests on pure ANF-PVA hydrogels and ANF-Fe_3O_4-PVA hydrogels with various concentrations of nanoparticles (Table S2). The magnetic composite hydrogels exhibit high strength (1.32-2.4 MPa) and stretchability (53.3%-66.6%) similar to those of pure ANF-PVA hydrogels (Figure 2c-e). However, the Fe_3O_4 nanoparticles functionalized with amine or hydroxyl groups might have a

slight interference with the hydrogen bonding between ANFs and PVA, which plays a significant role in the mechanical properties of the hydrogels. With lower nanoparticle concentrations (7.3 wt% or 13.7 wt% of dried samples), the fracture strains of ANF-Fe_3O_4-PVA hydrogels are similar to that of pure ANF-PVA hydrogel (Figure 2c). The energy dissipation characteristics of these ANF-Fe_3O_4-PVA hydrogels are also similar to those of pure ANF-PVA (Figure S7).[8] Samples with higher nanoparticle concentrations (24.1 wt% or 32.2 wt%) exhibit decreases in tensile strength and facture strain (Figure 2e). From SEM examination, all of the samples retain the 3D nanofiber network originating from the ANF framework (Figure 2f). Further optimization of the magnetic responses and mechanical properties of the composite hydrogels can be achieved by tuning the composition based on specific device applications.

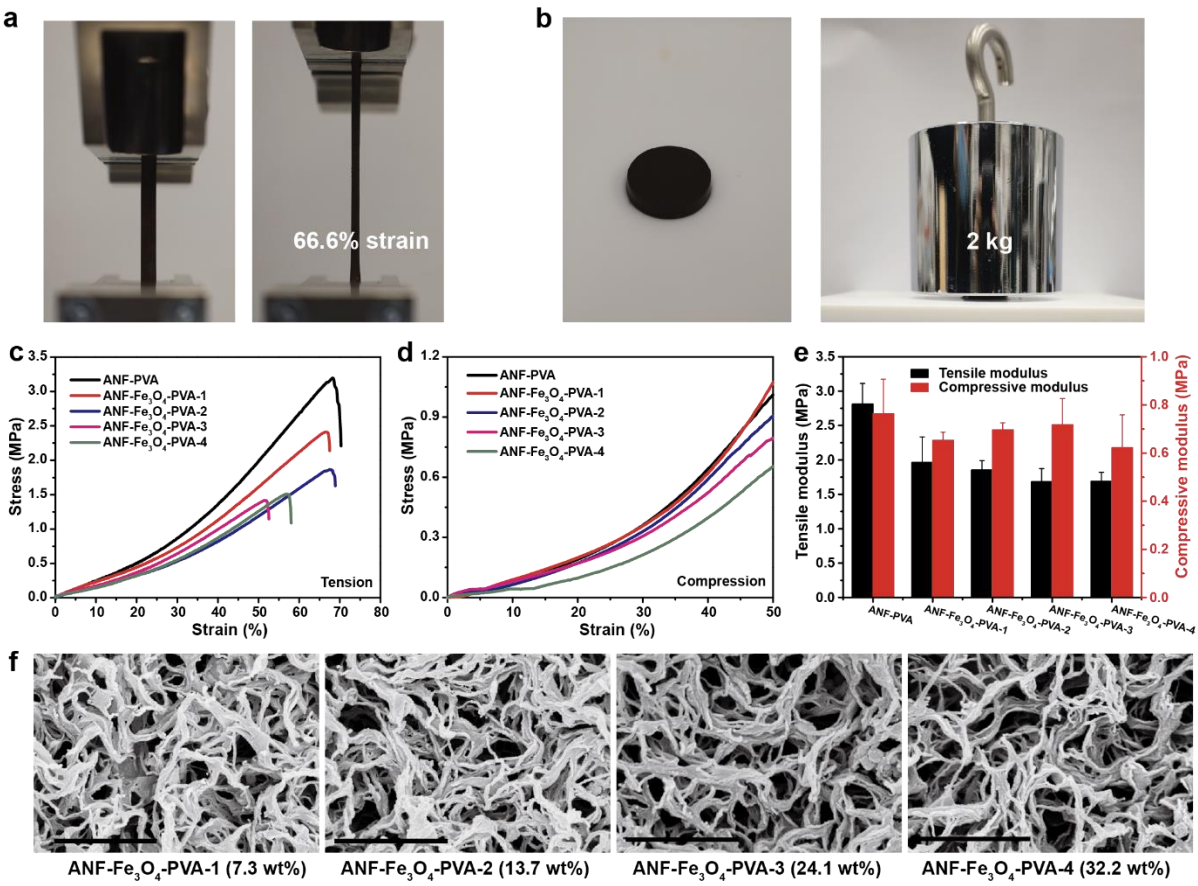

Figure 2. Mechanical properties of ANF-Fe_3O_4-PVA magnetic composite hydrogel. (a) Photographs showing a sample of ANF-Fe_3O_4-PVA-1 magnetic hydrogel with 0% (left) and 66.6% (right) tensile strains. (b) Photographs showing a sample of ANF-Fe_3O_4-PVA-1 magnetic hydrogel without (left) and with (right) a compressive load of 20 N (2 kg). (c-d) Uniaxial (c) tensile and (d) compressive stress–strain curves for ANF-PVA, and ANF-Fe_3O_4-PVA magnetic hydrogels with four concentrations. (e) Tensile and compressive moduli of various samples. (f) SEM images showing the morphology of ANF-Fe_3O_4-PVA hydrogel samples with increasing content of Fe_3O_4 nanoparticles (from ANF-Fe_3O_4-PVA-1 to ANF-Fe_3O_4-PVA-4). Scale bars: 1 μm.

The compressive behaviors of ANF-Fe_3O_4-PVA hydrogels are less dependent on the loading of nanoparticles (Figure 2d-e). Samples loaded with Fe_3O_4 nanoparticles retain similar compressive responses as the pure ANF-PVA hydrogels (Figure 2d). Different from the tensile responses that mostly arise from the nanofiber network, the compression resistance of the hydrogels is also related to the trapping of interstitial water flow that is less dependent of nanoparticle loading.[8] Overall, the mechanical robustness of the ANF-Fe_3O_4-PVA hydrogels is sufficient for device applications even with high loading of Fe_3O_4 nanoparticles.

Near-infrared (NIR) laser induced welding. Welding and fusing of functional hydrogels are important for the fabrication of hybrid devices or repairing of damaged structures. Existing processing methods for soft materials, including thermal annealing, solvent treatment, or chemical cross-linking, lack the capability in spatially selective welding.[36,37] In addition, given the good solvent stability and low thermal conductivity of ANFs combined with the water-rich feature of the matrix, these traditional methods are incapable of welding ANF-based composite

hydrogels. On the other hand, incorporation of photothermally active components may enable an approach to selective welding of ANF-based hydrogels. Typical photothermally active components are exemplified by organic dyes and gold nanoparticles,[38,39] but their incorporation into the ANF-PVA-Fe_3O_4 system may complicate the manufacturing process, increase the cost or impact the mechanical properties. Interestingly, the photothermal properties of Fe_3O_4 nanoparticles embedded in the PVA-rich composite hydrogels may enable a convenient method for selective welding through NIR laser irradiation.[40,41] Under the radiation of NIR laser with maximum power of 0.5 W, the temperature of the hydrogel ANF-Fe_3O_4-PVA-1 (7.3 wt% Fe_3O_4 nanoparticle loading) raised to 470 °C in 5 seconds as recorded by an infrared thermal imaging system (Figure 3a). This temperature rise, which also demonstrated in other samples (Figure S8), can be utilized to weld separate hydrogel strips and achieve high healing efficiency (Figure 3b-c). The rapid temperature elevation can be ascribed to the high density of Fe_3O_4 nanoparticles on the surface of nanofibers, which can be further confirmed by numerical simulation on an array of nanoparticles (Figure 3d-f). The center of the array displays a higher temperature than the end part under the illumination of the NIR laser, due to coupling of Fe_3O_4 nanoparticles. Moreover, the internal heating source dispersed within the hydrogel matrix is beneficial for the high temperature rise since the aramid-based materials have a low thermal conductivity.[22,42] Though significantly enhanced photothermal properties can be achieved by magnetic particle clusters[28–30], when designing nanoparticle-hydrogel systems, a balance between enhanced photothermal properties and overall homogeneity should be handled carefully. Twofold factors are considered: first, the aggregation of nanoparticles is irregular and uncontrollable due to their strong inter-particle interaction; second, such aggregation would induce structural failure or ununiform heating, resulting in reduced efficacy and even defects due to local overheating.

Investigations on the microscale morphology revealed the healing/welding process (Figure 3g). Under the NIR illumination, the elevated temperature enhances the fluidity of the fibrous nanocomposites, providing driving forces that bypass the kinetic traps and reduce the free interfacial energy. The nanofibers connect and merge as they are softened by elevated temperature. The water-rich protective PVA layer mitigates the high transient temperature that can damage the fibers and provides time window for operation. Further indicated by the change in external appearance of as-welded samples, the welding process results in densification of the networks. For thin film samples with 80 μm in thickness, the welded regions become more transparent, while the same regions for thick stripes (250 μm in thickness) exhibit obvious shrink (Figure 3b). As a comparison, ANF-Fe_3O_4 aerogels are easily burned by NIR laser, even under low laser intensity (Figure S9). By increasing the illumination time, two hydrogels are fused together, of which the interface becomes smooth but condensed.

The mechanical properties of healed hydrogels are dependent on the thickness of samples, as indicated by tensile tests (Figure S10a-b). Besides the homogenous welding of the same type of hydrogels, our method can also realize "macroscopic assembly" by welding the ANF-Fe_3O_4-PVA and ANF-PVA hydrogel, forming heterojunctions, as indicated by their distinct colors (Figure 1e-g, and S10c). Tensile stress-strain curves indicate 65.33% fracture strain is retained by the healed hydrogel sample, achieving a high healing efficiency of 98%, when comparing to the 66.60% fracture strain of the original hydrogel sample (Figure 3c). The heterojunction can resist up to 42.73% strain and 0.8385 MPa stress before fracture. Nonuniform nanoparticle distribution may cause insufficient heating at the interface, resulting in reduced healing efficiency. Compared with healed stripe samples that retain 94.8% tensile modulus and 98.09% fracture strain, thin films samples exhibit a significantly decreased healing efficiency in modulus

(79.4%) and strain (69.94%) (Figure S11). Since the healing process is protected by PVA and interstitial water, under the same healing time, thinner films may experience more damage due to lower water content. To optimize the healing efficiency, finding the balance between water content, nanoparticle concentration, and welding power would worth future investigations.

In addition, the hydrogels can be employed as soft ionic conductors with infiltrated sodium citrate. This conductive hydrogel is also healable using NIR induced welding, and electrical conductivity of the hydrogel is maintained even under bending and twisting (Figure 3h). In addition to Fe_3O_4 nanoparticles, we synthesized gold (Au) nanoparticles with a diameter of ~25 nm (Figure S12) to replace Fe_3O_4 nanoparticles for the fabrication of ANF-Au-PVA composite hydrogel (Figure S13), as gold nanoparticles are biocompatible[43] and exhibit good electrical conductivity.[44] The resistance change against strain exhibits a linear and monotonic increase when stretched up to 70%, the rupture strain of ANF-Au-PVA hydrogel. With gauge factor of 1.979, calculated by the resistance change divided by the strain, this linear trend shows a feasible electrical property as a strain sensor.

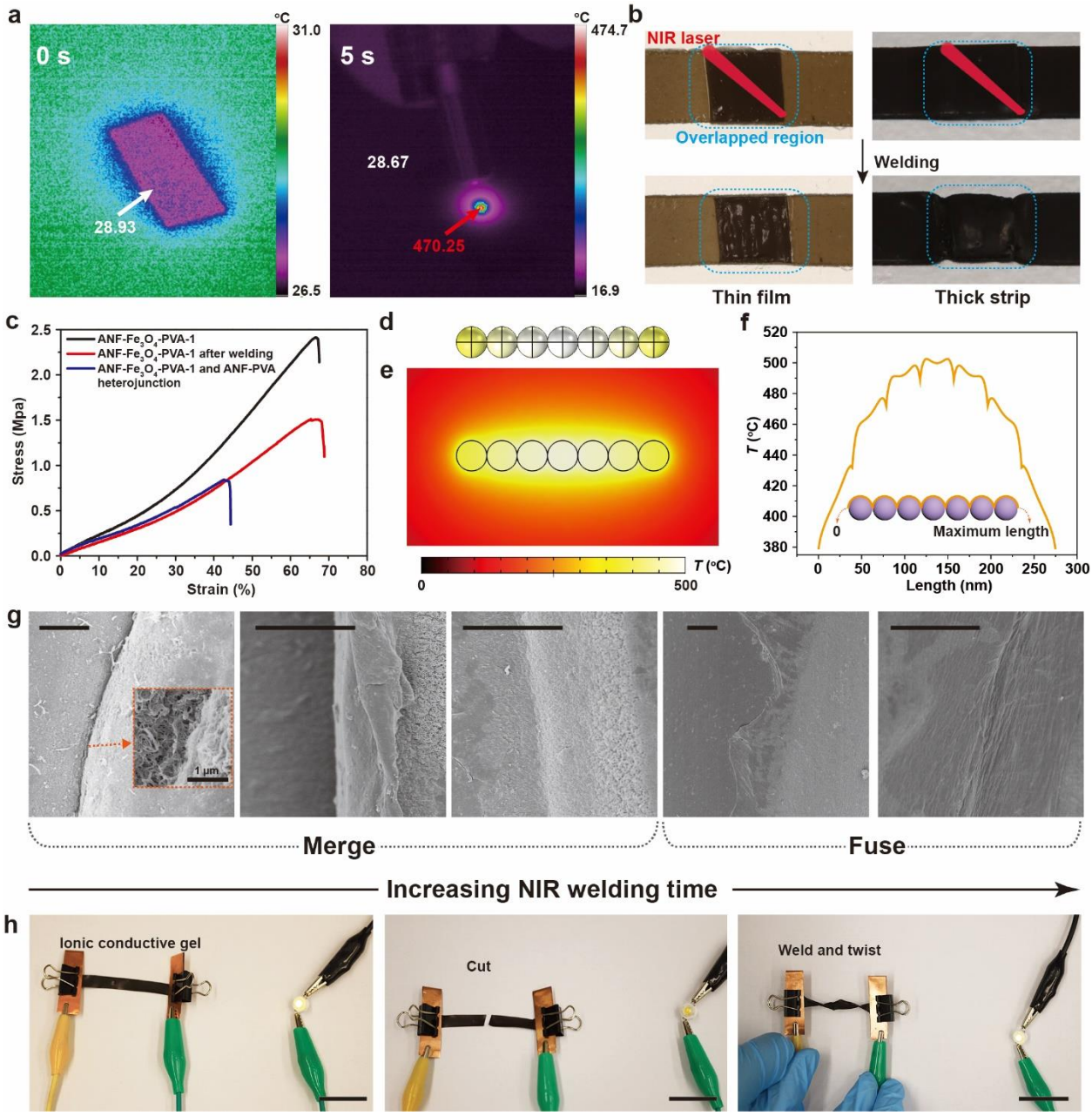

Figure 3. Photothermally induced welding of ANF-Fe_3O_4-PVA magnetic composite hydrogel. (a) Infrared images showing the temperature change of the hydrogel from 28.93 ºC to 470.25 ºC in 5 seconds under the illumination of a NIR laser. (b) Photographs showing the separated hydrogel thin films (left) and thick stripes (right) can be welded together by the NIR laser. (c) Stress–strain curves for the welded hydrogels. (d-e) Numerical simulation of (d) the spatial distribution of temperature on an array of Fe_3O_4 nanoparticles and (e) surrounding environment

under NIR laser irradiation. (f) Corresponding length-temperature plot showing temperature distribution on an array of Fe_3O_4 nanoparticles under NIR laser, where the center part of the array shows the highest temperature due to the coupling effect. (g) SEM images at different welding stages showing that the interfaces are experiencing merging processes, and finally fused together. Scale bars: 20 μm. (h) Photographs showing an LED powered through a conductive hydrogel sample before and after the cutting-healing process. Scale bars: 2 cm.

This unique approach to welding and healing aramid-based materials opens a new way for the improvement of device fabrication and materials recycling (Figure 4). First, the traditional method to recycle the aramid materials faces severe challenges, including high energy/solvent cost, harsh degradation conditions, and, specifically for aramid composites, expensive purification process. Our method provides a new idea to recycle ANFs forming desirable shapes with high energy efficiency and without solvent aided physical and/or chemical treatment.[45] Second, the ANFs have long been used as building blocks constructing highly connective networks as reinforcing components. It is not an easy task to dial in functionalities to such materials in a clickable manner or fabricate hybrid structures. In addition, the welding can be repeated multiple times without significant degradation of mechanical strength (Figure S14). Our strategy of heterogenous welding provides a customizable, modular approach that integrates various components with distinct functionalities.

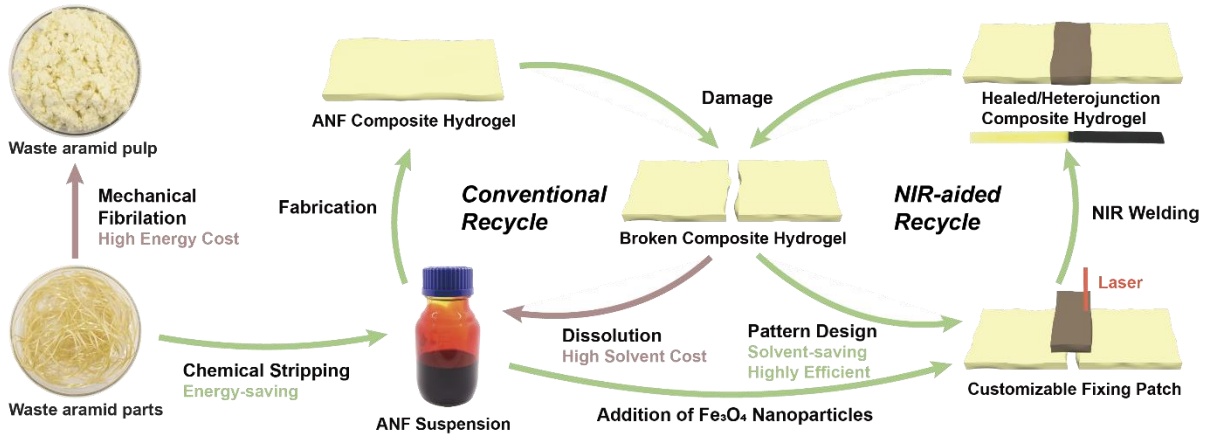

Figure 4. Schematics of various recycling processes of aramid materials, including those based on chemical stripping, mechanical fibrillation, and NIR-aided welding.

Soft programmable actuators. Due to the inherent magnetic nature of Fe_3O_4 nanoparticles (Figure S3a), the ANF-Fe_3O_4-PVA hydrogels can serve as programmable soft magnetic actuators (Figure S3b-c). Existing soft magnetic hydrogels usually achieve actuation patterns based on anisotropic assembly of magnetic nanoparticles with predesigned alignments.[1] However, the sophisticated assembly process may impose restrictions on device fabrication or mechanical performance. For ANF-Fe_3O_4-PVA hydrogels, due to their photothermal weldability, they can be integrated with non-magnetic ANF-PVA hydrogels and achieve modulated, controllable actuation patterns through hybrid structures (Figure 5a). Actuation experiments were performed using nine combined cylindrical magnets with total center magnetic field strength of 390 mT perpendicular to the operation plane under ambient conditions. The pure ANF-Fe_3O_4-PVA stripe exhibits a bending motion under magnetic field applied at one end (Figure 5b). To further demonstrate the magnetic actuation of the hydrogel samples, we tested the anisotropic responses of four hydrogel samples with heterojunctions under magnetic field applied at the central position (Figure 5c-e, Video S1-S2). Through different welding patterns, the actuators show different transformations, demonstrating the possibility of programmable and customizable

control. Our working principles also allow for the construction of more complex shapes and patterns. For example, a flower-shaped hydrogel is formed by ANF-Fe_3O_4-PVA petals and an ANF-PVA core, potentially serving as a reversible robotic hand for grasping objects (Figure 5f). Compared with other magnetic hydrogels based on self-healing strategies utilizing precursor loading, metal-coordination, hydrogen bonds,[46–48] *etc*., which are limited by sophisticated chemical processes and insufficient mechanical performance,[46,49] our methods exhibit a high healing efficiency, mechanical strength, and manufacturability that does not require complex chemical modifications.

The chemical stability of our hydrogels further limits hazardous waste production during polymer reconfiguration and shape morphing *via* photothermal effects, mechanical forces, and magnetic fields, ensuring a high degree of safety. This high stability of the hydrogels yields excellent biocompatibility even suitable for primary human cells such as chondrocytes. Though generally considered biologically safe,[3] studies have indicated that Fe_3O_4 nanoparticles' concentration, sizes, and their interaction with cells[50,51] influence the cytotoxicity. To further investigate the cytotoxicity and biocompatibility of the composite hydrogel, fibroblast cell line NIH/3T3, a major cell line in connective tissues, was cultured on the ANF-Fe_3O_4-PVA-1, ANF-Fe_3O_4-PVA-2, and ANF-Fe_3O_4-PVA-3 hydrogel samples without surface modification. From day 1 to day 5, no obvious difference is observed in cell viability (Figure 5g & S15). Though potential biocompatibility concerns may relate to high temperature rise, by controlling irradiation time and laser intensity, our magnetic hydrogel may also be utilized to perform photothermal therapy at a temperature level around 50 ^{o}C.[52,53]

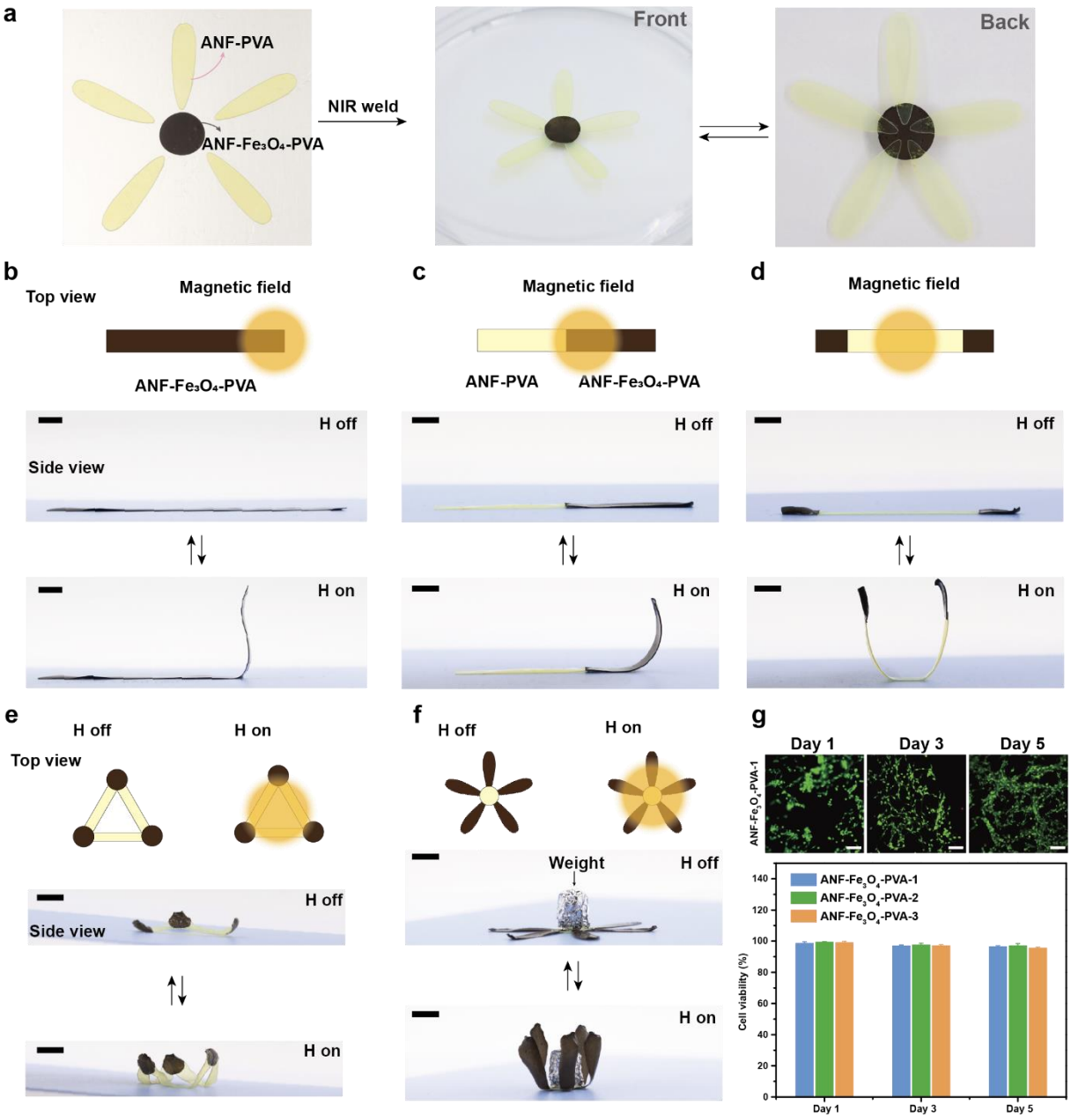

Figure 5. Magnetic actuation and biocompatibility of photothermally welded ANF-Fe_3O_4-PVA hydrogels. (a) Photographs showing the welding process of a flower-like heterostructure fabricated from ANF-Fe_3O_4-PVA and ANF-PVA hydrogels. (b-f) Photographs showing reversible actuation of hydrogel structures with (b) pure ANF-Fe_3O_4-PVA and heterostructures with (c) one, (d) two, or (e) three pieces of magnetic hydrogel patches, as well as (f) a complex flower-like structure. The actuation was induced by 9 magnets with total magnetic field strength

of 390 mT applied perpendicular to the plane. Each cylindrical magnet has a dimension of 20 × 5 mm. Scale bars: 4 mm. (g) Fluorescent images (top) and cell viability histogram (bottom) of fibroblasts cultured on ANF-Fe_3O_4-PVA magnetic composite hydrogel, measured on day 1, day 3, and day 5 after cell seeding. Scale bars: 100 μm.

CONCLUSIONS

In conclusion, we have introduced a facile and scalable approach to the fabrication of mechanically robust and magnetically active hydrogels with potential applications in soft robots and remotely controllable biomedical actuators. Using NIR welding methods, we can achieve custom designed heterogenous structures with possibility of complex modes of deformation. Our recent work has demonstrated the ability to integrate various microelectronic sensors and electroactive polymers onto ANF-PVA based materials.[21] In combination with the soft electronics, the multifunctional hydrogel platform may achieve more sophisticated sensing and actuation capabilities in a closed-loop manner. The hybrid device platform could enable diverse applications in implantable surgical tools, human-robot interactions, controlled release of drugs, photothermal therapies, and many other technologies.

METHODS

Synthesis of Fe_3O_4 nanoparticles with amine groups on the surface. To match the diameter of the aramid nanofibers (ANF), the Fe_3O_4 nanoparticles with 20-30 nm in diameter were synthesized *via* the reported strategy.[54] Briefly, 0.6 g of $FeCl_3$ as ferro source was dissolved with 6.5 g of 1,6-hexanediamine and 2.0 g anhydrous sodium acetate in 30 mL glycol by 50 °C vigorously stirring and sonification. The fully dissolved, transparent solution was transferred into

a Teflon-lined autoclave and put into oven at 198 ºC for 6 h. The magnetite nanoparticles were then washed by ethanol and DI water *via* magnet collection and dispersion process (2 to 3 times) to remove the residue reactant, and finally dispersed in DI water. Due to the strong dipolar interactions of magnetic particles, the particles tend to form clusters and even aggregate. The particles are then washed by DMSO (three times) through magnet induced precipitation and redispersion process, forming stable suspension prior to hydrogel fabrication. TEM (FEI Tecnai G2 20 Scanning TEM) is employed to characterize the nanoparticles. X-ray diffraction measurements were performed using a Cu Kα source (λ=1.541 Å, Rigaku SmartLab) in the 2θ range of 15-95° using scanning rate at 5° min^{-1}. To prepare the samples, the as-synthesized Fe_3O_4 nanoparticles were drop-casted onto the sample holder and dried at 60 °C under ambient condition before measurement. The magnetic characterization was performed on Fe_3O_4 nanoparticles, ANF-Fe_3O_4 composites, and ANF-Fe_3O_4-PVA hydrogels under magnetic field from -2T to 2T (Lakeshore VSM 7307).

Fabrication of ANF-Fe_3O_4-PVA hydrogel. ANF suspension (2 wt%) in DMSO was prepared using the reported method and mixed with the Fe_3O_4 DMSO suspension.[35] The mixing ratio can be varied by changing the concertation of nanoparticles, while the volume of the suspension keeps constant. The mixture was stirred vigorously for 2 minutes to ensure adequate assembly with the Fe_3O_4 particles through hydrogen bonding. Then a 10 wt% PVA DMSO solution with an equal volume to ANF suspension was added, followed by another 2 min of stirring. This process is highly water sensitive and should be performed under an inert environment such as nitrogen gas (in a glove box). Any water absorption will induce the microscale ANF gelation and lead to micro phase separation, which is detrimental for their mechanical performance. The mixture was either coated as film or cast in customized molds. The whole stirring and molding

processes were performed on a hot plate (80 ℃, with magnet) to maintain the good fluidity. The shaped mixture was then immersed in DI water to generate ANF-Fe_3O_4-PVA hydrogel. Fabrication procedures for ANF-PVA and ANF-Au-PVA hydrogels are the same, where ANF-PVA hydrogels do not require addition of nanoparticles, and ANF-Au-PVA hydrogels adds Au particles instead of Fe_3O_4. For SEM (Hitachi S4800 FEG SEM) characterization, supercritical CO_2 drying was employed to remove water from the hydrogel matrix without further damage.

Mechanical test of ANF-Fe_3O_4-PVA hydrogel. The mechanical tests were performed under ambient condition using a universal testing machine (Zwick Roell, German). For tensile tests, thick (250 μm) and thin (80 μm) rectangular strips with 5 mm in width and 6 cm in length were prepared using laser cutting machine and tested under strain rate at 100%/min. For compression test, cylindrical samples with 10 mm diameter and 3 mm in thickness were prepared by pouring and degassing mixed solution into Teflon molds. The compression tests were performed under strain rate at 100%/min. For healed samples, the tensile tests were performed under strain rate at 100%/min.

NIR induced welding of ANF-Fe_3O_4-PVA hydrogel. Prior to NIR welding, the ANF-Fe_3O_4-PVA hydrogel samples were fabricated in bulk by doctor blade coating method. After solvent exchange process, the hydrogel samples were laser cut into desired shapes. The NIR welding is realized by the photothermal effect of Fe_3O_4 nanoparticles. Two pieces of ANF-Fe_3O_4-PVA hydrogel films with the same width were overlapped along their long axis, followed by the NIR laser illumination (785-nm, Shanghai Laser & Optics Century, IRM785RMA-300FC). The NIR power and welding duration rely on the thickness of films and the demand of mechanical strength at the joint, both enhancing the NIR power and extending the welding duration result in denser and stronger joints.

Magnetic actuation experiments. The actuation was induced by 9 cylindrical magnets with total magnetic field strength of 390 mT applied perpendicular to the plane. Each cylindrical magnet has a dimension of 20 × 5 mm. Here, the as-prepared patterned hydrogel samples were laid on a plane, and the magnet set was held upright and moved to approach the sample for actuation behavior.

Cell culture and fluorescence characterization. The hydrogel samples were cut and washed with ethanol and phosphate buffered saline (Gibco™ pH 7.4 basic (1x)) prior to cell culture. Dulbecco's modified eagle medium (DMEM, Gibco™, high glucose), fetal bovine serum (Gibco™, qualified, Brazil), and Penicillin-Streptomycin (Gibco™, 10,000 U/mL) were mixed as received at 89%, 10%, 1% in volume fraction, respectively. Mouse embryonic fibroblast NIH 3T3 were cultured. And the samples were characterized on day 1, 3, and 5 during culturing. To characterize the samples, LIVE/DEAD™ Cell Imaging Kit (488/570) (Invitrogen™) were used as received, the cells were treated for 15 min under ambient room conditions. The florescence was characterized using Nikon Eclipse Ci-L.

Numerical simulation. COMSOL Multiphysics (version 5.4a) was used to simulate the temperature on and around light-heated particles. Seven closely attached Fe_3O_4 nanoparticles with a diameter of 25 nm were placed in a 1000 nm × 1000 nm × 1000 nm box filled with hydrogel as media. The model involves modules of heat transfer in solids.

$$\nabla \cdot \boldsymbol{q} = Q$$

$$\boldsymbol{q} = -k\nabla T$$

where $\boldsymbol{q}$ is the heat flux vector, Q is heating source power, T is temperature, and k is thermal conductivity. The upper half surface of spherical particles was endowed with boundary heat source, which mimics light heating.

$$-\boldsymbol{n} \cdot \boldsymbol{q} = Q_b$$

The $\boldsymbol{n}$ is boundary normal vector. The boundary source power, Q_b, was set as 1.810 Wm^{-2}. The sides of the box were set to be at room temperature, 293.15 K. Due to the high-water content, the hydrogel was regarded to have same heat transfer properties as deionized water, possessing a thermal conductivity, 0.59 $Wm^{-1}K^{-1}$, while the thermal conductivity of Fe_3O_4 nanoparticles was set as 5.9 $Wm^{-1}K^{-1}$. After these settings, the model can simulate the temperature distribution on and around particles, where we found the central part of the nanoparticle array to be more heated.

ASSOCIATED CONTENT

Supporting Information. The following files are available free of charge. Synthesis of Au nanoparticles; photographs of processing of ANF-Fe_3O_4-PVA hydrogels; electron diffraction pattern, X-ray diffraction pattern of Fe_3O_4 nanoparticles; magnetic hysteresis curves of Fe_3O_4 nanoparticles, ANF-Fe_3O_4 nanocomposite, and ANF-Fe_3O_4-PVA hydrogels; photographs of nanoparticle suspension stability; table for material composition of ANF-Fe_3O_4-PVA hydrogels; cyclic tensile and compression tests of magnetic hydrogels; near-infrared images of ANF-Fe_3O_4-PVA hydrogels heated by near-infrared laser; SEM images of burned ANF-Fe_3O_4 aerogel; photographs of a stretching process applied on welded hydrogel samples; mechanical tests comparison of tensile stress and strain at break between ANF-Fe_3O_4-PVA-1 hydrogels and the same hydrogels experienced cut-welding process; photographs and sensitivity test of ANF-Au-PVA composite hydrogel as a strain sensor; mechanical tests on heterojunction hydrogels after secondary welding; fluorescence microscope images of fibroblasts cultured on ANF-Fe_3O_4-PVA magnetic composite hydrogels (PDF)

Video for actuation of hydrogel heterostructures with one pieces of magnetic hydrogel patches (MP4)

Video for actuation of hydrogel heterostructures with two pieces of magnetic hydrogel patches (MP4)

AUTHOR INFORMATION

Corresponding Author

*Department of Mechanical Engineering, The University of Hong Kong, Hong Kong SAR 999077, China. Email Address: xulizhi@hku.hk

Present Addresses

†Department of Materials Science and Engineering and Materials Research Laboratory, University of Illinois at Urbana-Champaign, Urbana, IL, USA

Author Contributions

Zuochen W. conceived the research. Zuochen W., H.Z., H.L., and B.Y. planned the experiments. L.W. and L.X. supervised the research. Zuochen W. and H.Z. prepared the samples. H.Z. carried out actuation and cell experiments. M.S. carried out mechanical tests. Zhisheng W. and Y.W. carried out numerical simulation and discussed nanoparticle synthesis. L.X., Z.W., and H.Z. co-wrote the manuscript with assistance from the other authors. ‡These authors contributed equally: Zuochen Wang and Hengjia Zhu.

Funding Sources

The study is supported by the Research Grants Council (RGC), the University Grants Committee (UGC) (Project 17200722 and 17200320 to L.X.; GRF 17205421, 17204420, 17210319, 17204718, and CRF C1006-20WF to L.W.).

Notes

The authors declare no conflict of interest.

ACKNOWLEDGMENT

The study is supported by the Research Grants Council (RGC), the University Grants Committee (UGC) (Project 17200722 and 17200320 to L.X.; GRF 17205421, 17204420, 17210319, 17204718, and CRF C1006-20WF to L.W.). The authors thank Hongzhen Liu for his help in providing ANF materials and contribution to sample fabrication.

REFERENCES

(1) Kim, Y.; Zhao, X. Magnetic Soft Materials and Robots. *Chem. Rev.* **2022**, *122* (5), 5317–5364.

(2) Liu, X.; Liu, J.; Lin, S.; Zhao, X. Hydrogel Machines. *Mater. Today* **2020**, *36*, 102–124.

(3) Pardo, A.; Gómez-Florit, M.; Barbosa, S.; Taboada, P.; Domingues, R. M. A.; Gomes, M. E. Magnetic Nanocomposite Hydrogels for Tissue Engineering: Design Concepts and Remote Actuation Strategies to Control Cell Fate. *ACS Nano* **2021**, *15* (1), 175–209.

(4) Hu, W.; Lum, G. Z.; Mastrangeli, M.; Sitti, M. Small-Scale Soft-Bodied Robot with Multimodal Locomotion. *Nature* **2018**, *554* (7690), 81–85.

(5) Kim, Y.; Yuk, H.; Zhao, R.; Chester, S. A.; Zhao, X. Printing Ferromagnetic Domains for Untethered Fast-Transforming Soft Materials. *Nature* **2018**, *558* (7709), 274–279.

(6) Song, H.; Lee, H.; Lee, J.; Choe, J. K.; Lee, S.; Yi, J. Y.; Park, S.; Yoo, J.-W.; Kwon, M. S.; Kim, J. Reprogrammable Ferromagnetic Domains for Reconfigurable Soft Magnetic Actuators. *Nano Lett.* **2020**, *20* (7), 5185–5192.

(7) Xu, T.; Zhang, J.; Salehizadeh, M.; Onaizah, O.; Diller, E. Millimeter-Scale Flexible Robots with Programmable Three-Dimensional Magnetization and Motions. *Sci. Robot.* **2019**, *4* (29), eaav4494.

(8) Xu, L.; Zhao, X.; Xu, C.; Kotov, N. A. Water-Rich Biomimetic Composites with Abiotic Self-Organizing Nanofiber Network. *Adv. Mater.* **2018**, *30* (1), 1703343.

(9) Pardo, A.; Bakht, S. M.; Gomez-Florit, M.; Rial, R.; Monteiro, R. F.; Teixeira, S. P. B.; Taboada, P.; Reis, R. L.; Domingues, R. M. A.; Gomes, M. E. Magnetically-Assisted 3D Bioprinting of Anisotropic Tissue-Mimetic Constructs. *Adv. Funct. Mater.* **2022**, *32* (50), 2208940.

(10) Rodríguez-Velázquez, E.; Silva, M.; Taboada, P.; Mano, J. F.; Suárez-Quintanilla, D.; Alatorre-Meda, M. Enhanced Cell Affinity of Chitosan Membranes Mediated by Superficial Cross-Linking: A Straightforward Method Attainable by Standard Laboratory Procedures. *Biomacromolecules* **2014**, *15* (1), 291–301.

(11) Liu, X.; Yang, Y.; Inda, M. E.; Lin, S.; Wu, J.; Kim, Y.; Chen, X.; Ma, D.; Lu, T. K.; Zhao, X. Magnetic Living Hydrogels for Intestinal Localization, Retention, and Diagnosis. *Adv. Funct. Mater.* **2021**, *31* (27), 2010918.

(12) Zhang, Y.; Chen, S.; Xiao, Z.; Liu, X.; Wu, C.; Wu, K.; Liu, A.; Wei, D.; Sun, J.; Zhou, L.; Fan, H. Magnetoelectric Nanoparticles Incorporated Biomimetic Matrix for Wireless Electrical Stimulation and Nerve Regeneration. *Adv. Healthc. Mater.* **2021**, *10* (16), 2100695.

(13) Zhao, X.; Chen, X.; Yuk, H.; Lin, S.; Liu, X.; Parada, G. Soft Materials by Design: Unconventional Polymer Networks Give Extreme Properties. *Chem. Rev.* **2021**, *121* (8), 4309–4372.

(14) Bonhome-Espinosa, A. B.; Campos, F.; Rodriguez, I. A.; Carriel, V.; Marins, J. A.; Zubarev, A.; Duran, J. D. G.; Lopez-Lopez, M. T. Effect of Particle Concentration on the Microstructural and Macromechanical Properties of Biocompatible Magnetic Hydrogels. *Soft Matter* **2017**, *13* (16), 2928–2941.

(15) Mao, L.-B.; Gao, H.-L.; Yao, H.-B.; Liu, L.; Cölfen, H.; Liu, G.; Chen, S.-M.; Li, S.-K.; Yan, Y.-X.; Liu, Y.-Y.; Yu, S.-H. Synthetic Nacre by Predesigned Matrix-Directed Mineralization. *Science* **2016**, *354* (6308), 107–110.

(16) Haider, H.; Yang, C. H.; Zheng, W. J.; Yang, J. H.; Wang, M. X.; Yang, S.; Zrínyi, M.; Osada, Y.; Suo, Z.; Zhang, Q.; Zhou, J.; Chen, Y. M. Exceptionally Tough and Notch-Insensitive Magnetic Hydrogels. *Soft Matter* **2015**, *11* (42), 8253–8261.

(17) Lee, J. H.; Han, W. J.; Jang, H. S.; Choi, H. J. Highly Tough, Biocompatible, and Magneto-Responsive Fe_3O_4/Laponite/PDMAAm Nanocomposite Hydrogels. *Sci. Rep.* **2019**, *9* (1), 15024.

(18) Zhao, Z.; Fang, R.; Rong, Q.; Liu, M. Bioinspired Nanocomposite Hydrogels with Highly Ordered Structures. *Adv. Mater.* **2017**, *29* (45), 1703045.

(19) Mredha, Md. T. I.; Guo, Y. Z.; Nonoyama, T.; Nakajima, T.; Kurokawa, T.; Gong, J. P. A Facile Method to Fabricate Anisotropic Hydrogels with Perfectly Aligned Hierarchical Fibrous Structures. *Adv. Mater.* **2018**, *30* (9), 1704937.

(20) He, H.; Wei, X.; Yang, B.; Liu, H.; Sun, M.; Li, Y.; Yan, A.; Tang, C. Y.; Lin, Y.; Xu, L. Ultrastrong and Multifunctional Aerogels with Hyperconnective Network of Composite Polymeric Nanofibers. *Nat. Commun.* **2022**, *13* (1), 4242.

(21) Liu, H.; Li, H.; Wang, Z.; Wei, X.; Zhu, H.; Sun, M.; Lin, Y.; Xu, L. Robust and Multifunctional Kirigami Electronics with a Tough and Permeable Aramid Nanofiber Framework. *Adv. Mater.* **2022**, *34* (50), 2207350.

(22) Yang, B.; Wang, L.; Zhang, M.; Luo, J.; Lu, Z.; Ding, X. Fabrication, Applications, and Prospects of Aramid Nanofiber. *Adv. Funct. Mater.* **2020**, *30* (22), 2000186.

(23) He, H.; Li, Y.; Liu, H.; Kim, Y.; Yan, A.; Xu, L. Elastic, Conductive, and Mechanically Strong Hydrogels from Dual-Cross-Linked Aramid Nanofiber Composites. *ACS Appl. Mater. Interfaces* **2021**, *13* (6), 7539–7545.

(24) Yang, M.; Cao, K.; Sui, L.; Qi, Y.; Zhu, J.; Waas, A.; Arruda, E. M.; Kieffer, J.; Thouless, M. D.; Kotov, N. A. Dispersions of Aramid Nanofibers: A New Nanoscale Building Block. *ACS Nano* **2011**, *5* (9), 6945–6954.

(25) Lyu, J.; Wang, X.; Liu, L.; Kim, Y.; Tanyi, E. K.; Chi, H.; Feng, W.; Xu, L.; Li, T.; Noginov, M. A.; Uher, C.; Hammig, M. D.; Kotov, N. A. High Strength Conductive Composites with Plasmonic Nanoparticles Aligned on Aramid Nanofibers. *Adv. Funct. Mater.* **2016**, *26* (46), 8435–8445.

(26) Wang, L.; Zhang, M.; Yang, B.; Tan, J.; Ding, X. Highly Compressible, Thermally Stable, Light-Weight, and Robust Aramid Nanofibers/Ti_3AlC_2 MXene Composite Aerogel for Sensitive Pressure Sensor. *ACS Nano* **2020**, *14* (8), 10633–10647.

(27) Shen, S.; Wang, S.; Zheng, R.; Zhu, X.; Jiang, X.; Fu, D.; Yang, W. Magnetic Nanoparticle Clusters for Photothermal Therapy with Near-Infrared Irradiation. *Biomaterials* **2015**, *39*, 67–74.

(28) Nicolas-Boluda, A.; Yang, Z.; Guilbert, T.; Fouassier, L.; Carn, F.; Gazeau, F.; Pileni, M. P. Self-Assemblies of Fe_3O_4 Nanocrystals: Toward Nanoscale Precision of Photothermal Effects in the Tumor Microenvironment. *Adv. Funct. Mater.* **2021**, *31* (4), 2006824.

(29) Zhang, X.; Xu, X.; Li, T.; Lin, M.; Lin, X.; Zhang, H.; Sun, H.; Yang, B. Composite Photothermal Platform of Polypyrrole-Enveloped Fe3O4 Nanoparticle Self-Assembled Superstructures. *ACS Appl. Mater. Interfaces* **2014**, *6* (16), 14552–14561.

(30) Sun, M.; Li, H.; Hou, Y.; Huang, N.; Xia, X.; Zhu, H.; Xu, Q.; Lin, Y.; Xu, L. Multifunctional Tendon-Mimetic Hydrogels. *Sci. Adv.* **2023**, *9* (7), eade6973.

(31) Xue, J.; Wu, T.; Dai, Y.; Xia, Y. Electrospinning and Electrospun Nanofibers: Methods, Materials, and Applications. *Chem. Rev.* **2019**, *119* (8), 5298–5415.

(32) Pardo, A.; Yáñez, S.; Piñeiro, Y.; Iglesias-Rey, R.; Al-Modlej, A.; Barbosa, S.; Rivas, J.; Taboada, P. Cubic Anisotropic Co- and Zn-Substituted Ferrite Nanoparticles as Multimodal Magnetic Agents. *ACS Appl. Mater. Interfaces* **2020**, *12* (8), 9017–9031.

(33) *Nanooncology: Engineering Nanomaterials for Cancer Therapy and Diagnosis*; Gonçalves, G., Tobias, G., Eds.; Nanomedicine and Nanotoxicology; Springer International Publishing: Cham, 2018.

(34) Pardo, A.; Pelaz, B.; Gallo, J.; Bañobre-López, M.; Parak, W. J.; Barbosa, S.; del Pino, P.; Taboada, P. Synthesis, Characterization, and Evaluation of Superparamagnetic Doped Ferrites as Potential Therapeutic Nanotools. *Chem. Mater.* **2020**, *32* (6), 2220–2231.

(35) Zhu, J.; Yang, M.; Emre, A.; Bahng, J. H.; Xu, L.; Yeom, J.; Yeom, B.; Kim, Y.; Johnson, K.; Green, P.; Kotov, N. A. Branched Aramid Nanofibers. *Angew. Chem. Int. Ed.* **2017**, *56* (39), 11744–11748.

(36) Wu, T.; Li, H.; Xue, J.; Mo, X.; Xia, Y. Photothermal Welding, Melting, and Patterned Expansion of Nonwoven Mats of Polymer Nanofibers for Biomedical and Printing Applications. *Angew. Chem. Int. Ed.* **2019**, *58* (46), 16416–16421.

(37) Qian, Q.; Wang, J.; Yan, F.; Wang, Y. A Photo-Annealing Approach for Building Functional Polymer Layers on Paper. *Angew. Chem. Int. Ed.* **2014**, *53* (17), 4465–4468.

(38) Villar-Alvarez, E.; Leal, B. H.; Cambón, A.; Pardo, A.; Martínez-Gonzalez, R.; Fernández-Vega, J.; Al-Qadi, S.; Mosquera, V. X.; Bouzas, A.; Barbosa, S.; Taboada, P. Triggered RNAi Therapy Using Metal Inorganic Nanovectors. *Mol. Pharm.* **2019**, *16* (8), 3374–3385.

(39) Villar-Alvarez, E.; Cambón, A.; Pardo, A.; Arellano, L.; Marcos, A. V.; Pelaz, B.; del Pino, P.; Bouzas Mosquera, A.; Mosquera, V. X.; Almodlej, A.; Prieto, G.; Barbosa, S.; Taboada, P. Combination of Light-Driven Co-Delivery of Chemodrugs and Plasmonic-Induced

Heat for Cancer Therapeutics Using Hybrid Protein Nanocapsules. *J. Nanobiotechnology* **2019**, *17* (1), 106.

(40) Sadat, M. E.; Kaveh Baghbador, M.; Dunn, A. W.; Wagner, H. P.; Ewing, R. C.; Zhang, J.; Xu, H.; Pauletti, G. M.; Mast, D. B.; Shi, D. Photoluminescence and Photothermal Effect of Fe3O4 Nanoparticles for Medical Imaging and Therapy. *Appl. Phys. Lett.* **2014**, *105* (9), 091903.

(41) Chu, M.; Shao, Y.; Peng, J.; Dai, X.; Li, H.; Wu, Q.; Shi, D. Near-Infrared Laser Light Mediated Cancer Therapy by Photothermal Effect of Fe_3O_4 Magnetic Nanoparticles. *Biomaterials* **2013**, *34* (16), 4078–4088.

(42) Hu, Y.; Yang, G.; Zhou, J.; Li, H.; Shi, L.; Xu, X.; Cheng, B.; Zhuang, X. Proton Donor-Regulated Mechanically Robust Aramid Nanofiber Aerogel Membranes for High-Temperature Thermal Insulation. *ACS Nano* **2022**, *16* (4), 5984–5993.

(43) Kus-Liśkiewicz, M.; Fickers, P.; Ben Tahar, I. Biocompatibility and Cytotoxicity of Gold Nanoparticles: Recent Advances in Methodologies and Regulations. *Int. J. Mol. Sci.* **2021**, *22* (20), 10952.

(44) Huang, C.; Yao, Y.; Montes-García, V.; Stoeckel, M.; Von Holst, M.; Ciesielski, A.; Samorì, P. Highly Sensitive Strain Sensors Based on Molecules–Gold Nanoparticles Networks for High-Resolution Human Pulse Analysis. *Small* **2021**, *17* (8), 2007593.

(45) Yang, B.; Li, W.; Zhang, M.; Wang, L.; Ding, X. Recycling of High-Value-Added Aramid Nanofibers from Waste Aramid Resources via a Feasible and Cost-Effective Approach. *ACS Nano* **2021**, *15* (4), 7195–7207.

(46) Qi, M.; Yang, R.; Wang, Z.; Liu, Y.; Zhang, Q.; He, B.; Li, K.; Yang, Q.; Wei, L.; Pan, C.; Chen, M. Bioinspired Self-Healing Soft Electronics. *Adv. Funct. Mater.* **2023**, 2214479.

(47) Gao, X.; Deng, T.; Huang, X.; Yu, M.; Li, D.; Lin, J.; Yu, C.; Tang, C.; Huang, Y. Porous Boron Nitride Nanofibers as Effective Nanofillers for Poly(Vinyl Alcohol) Composite Hydrogels with Excellent Self-Healing Performances. *Soft Matter* **2022**, *18* (4), 859–866.

(48) Wang, S.; Urban, M. W. Self-Healing Polymers. *Nat. Rev. Mater.* **2020**, *5* (8), 562–583.

(49) Qin, H.; Zhang, T.; Li, N.; Cong, H.-P.; Yu, S.-H. Anisotropic and Self-Healing Hydrogels with Multi-Responsive Actuating Capability. *Nat. Commun.* **2019**, *10* (1), 2202.

(50) Coradeghini, R.; Gioria, S.; García, C. P.; Nativo, P.; Franchini, F.; Gilliland, D.; Ponti, J.; Rossi, F. Size-Dependent Toxicity and Cell Interaction Mechanisms of Gold Nanoparticles on Mouse Fibroblasts. *Toxicol. Lett.* **2013**, *217* (3), 205–216.

(51) Tishkevich, D. I.; Korolkov, I. V.; Kozlovskiy, A. L.; Anisovich, M.; Vinnik, D. A.; Ermekova, A. E.; Vorobjova, A. I.; Shumskaya, E. E.; Zubar, T. I.; Trukhanov, S. V.; Zdorovets, M. V.; Trukhanov, A. V. Immobilization of Boron-Rich Compound on Fe_3O_4 Nanoparticles: Stability and Cytotoxicity. *J. Alloys Compd.* **2019**, *797*, 573–581.

(52) Guedes, G.; Wang, S.; Fontana, F.; Figueiredo, P.; Lindén, J.; Correia, A.; Pinto, R. J. B.; Hietala, S.; Sousa, F. L.; Santos, H. A. Dual-Crosslinked Dynamic Hydrogel Incorporating Mo154 with PH and NIR Responsiveness for Chemo-Photothermal Therapy. *Adv. Mater.* **2021**, *33* (40), 2007761.

(53) Yuan, P.; Yang, T.; Liu, T.; Yu, X.; Bai, Y.; Zhang, Y.; Chen, X. Nanocomposite Hydrogel with NIR/Magnet/Enzyme Multiple Responsiveness to Accurately Manipulate Local Drugs for on-Demand Tumor Therapy. *Biomaterials* **2020**, *262*, 120357.

(54) Wang, L.; Bao, J.; Wang, L.; Zhang, F.; Li, Y. One-Pot Synthesis and Bioapplication of Amine-Functionalized Magnetite Nanoparticles and Hollow Nanospheres. *Chem. Eur. J.* **2006**, *12* (24), 6341–6347.

TABLE Of CONTENTS GRAPHIC